

## Article

# Physical Modeling for Large-Scale Landslide with Chair-Shaped Bedrock Surfaces under Precipitation and Reservoir Water Fluctuation Conditions

Shangtao Pan <sup>1,2,3</sup> , Wei Gao <sup>4,\*</sup> and Ruilin Hu <sup>1,2,3</sup>

<sup>1</sup> Key Laboratory of Shale Gas and Geoen지니어ing, Institute of Geology and Geophysics, Chinese Academy of Sciences, Beijing 100029, China; hb200302@163.com (S.P.); hurl@mail.iggcas.ac.cn (R.H.)

<sup>2</sup> Institutions of Earth Science, Chinese Academy of Sciences, Beijing 100029, China

<sup>3</sup> College of Earth and Planetary Sciences, University of Chinese Academy of Sciences, Beijing 100049, China

<sup>4</sup> China Earthquake Disaster Prevention Center, China Earthquake Administration, Beijing 100029, China

\* Correspondence: vera\_gao@foxmail.com

**Abstract:** The deformation and failure mechanisms of historical landslides, characterized with different types of bedrock surface shapes which are known to have been induced by rainfall and reservoir water fluctuations, is an important issue currently being addressed by many researchers. The Zhaoshuling Landslide of the Three Gorges Reservoir Region, which was characterized with a chair-shaped bedrock surface under rainfall and reservoir water fluctuation conditions, was selected as an example in this study's physical modeling process. The results of different parameters, including the displacements, pore water pressure, and total soil pressure during the landslide event, revealed that the Zhaoshuling Landslide with a chair-shaped bedrock surface had been extremely sensitive to heavy rainfall coupled with the rapid lowering of the water levels. Then, based on the data analysis results of the monitoring of the rainfall and groundwater levels, as well as the reservoir water levels, a conceptual model was put forward to explain the failure mechanisms. It was believed that the chair-shaped bedrock at the toe of the slope had been subjected to a localized zone of high transient pore water pressure, which had significantly adverse effects on the mechanisms of the slope stability.

**Keywords:** physical modeling; chair-shaped bedrock surface; pore water pressure; rainfall; reservoir water fluctuation conditions



**Citation:** Pan, S.; Gao, W.; Hu, R. Physical Modeling for Large-Scale Landslide with Chair-Shaped Bedrock Surfaces under Precipitation and Reservoir Water Fluctuation Conditions. *Water* **2022**, *14*, 984. <https://doi.org/10.3390/w14060984>

Academic Editors: Xingwei Ren, Zili Dai and Fangzhou Liu

Received: 15 February 2022

Accepted: 17 March 2022

Published: 21 March 2022

**Publisher's Note:** MDPI stays neutral with regard to jurisdictional claims in published maps and institutional affiliations.



**Copyright:** © 2022 by the authors. Licensee MDPI, Basel, Switzerland. This article is an open access article distributed under the terms and conditions of the Creative Commons Attribution (CC BY) license (<https://creativecommons.org/licenses/by/4.0/>).

## 1. Introduction

China's Three Gorges Region covers 193 km of the middle reaches of the Yangtze River between Fengjie in Chongqing City and Yichang in Hubei Province (as shown in Figure 1). Due to the steep valley-side slopes and long periods of river incision, a large number of landslides have been formed in the Three Gorges Reservoir area, of which more than 90% have been reactivated ancient landslides [1,2]. The Qianjiangping Landslide, which is a famous historical landslide, was reactivated at first by tentative impoundment combined with heavy rainfall and collapsed on July 14th of 2003. This disaster event resulted in major losses of lives and property [3–5]. The Liangshuijing Landslide in Yunyang, which is another ancient landslide, had also displayed intensified deformations in April of 2009, threatening many households located on the sliding body, as well as the shipping processes of the Yangtze River [6–8]. In order to prevent such tragedies and danger risks in the future, examinations of the potential revivals of ancient landslides in reservoir areas have received increasing attention in the field of engineering geology and geotechnical mechanics.

At the present time, the revival factors of historical landslides in the Three Gorges Reservoir area have mainly focused on the external inducing factors and the internal controlling factors. The rise and fall of reservoir water and rainfall levels are considered to be the most important inducing factors for the reactivations of ancient landslides in the reservoir area. The groundwater seepage and dynamic changes of groundwater levels

resulting from the rise and fall of reservoir water levels are of particular concern. The fluctuations in water levels tend to change the physical and mechanical properties of a region, as well as the stress state and stability of the slope material [9–13]. In addition, such internal controlling factors as topography, lithology, permeability, and material composition also play vital roles in the stability of an area prone to landslide events [5,14–16].

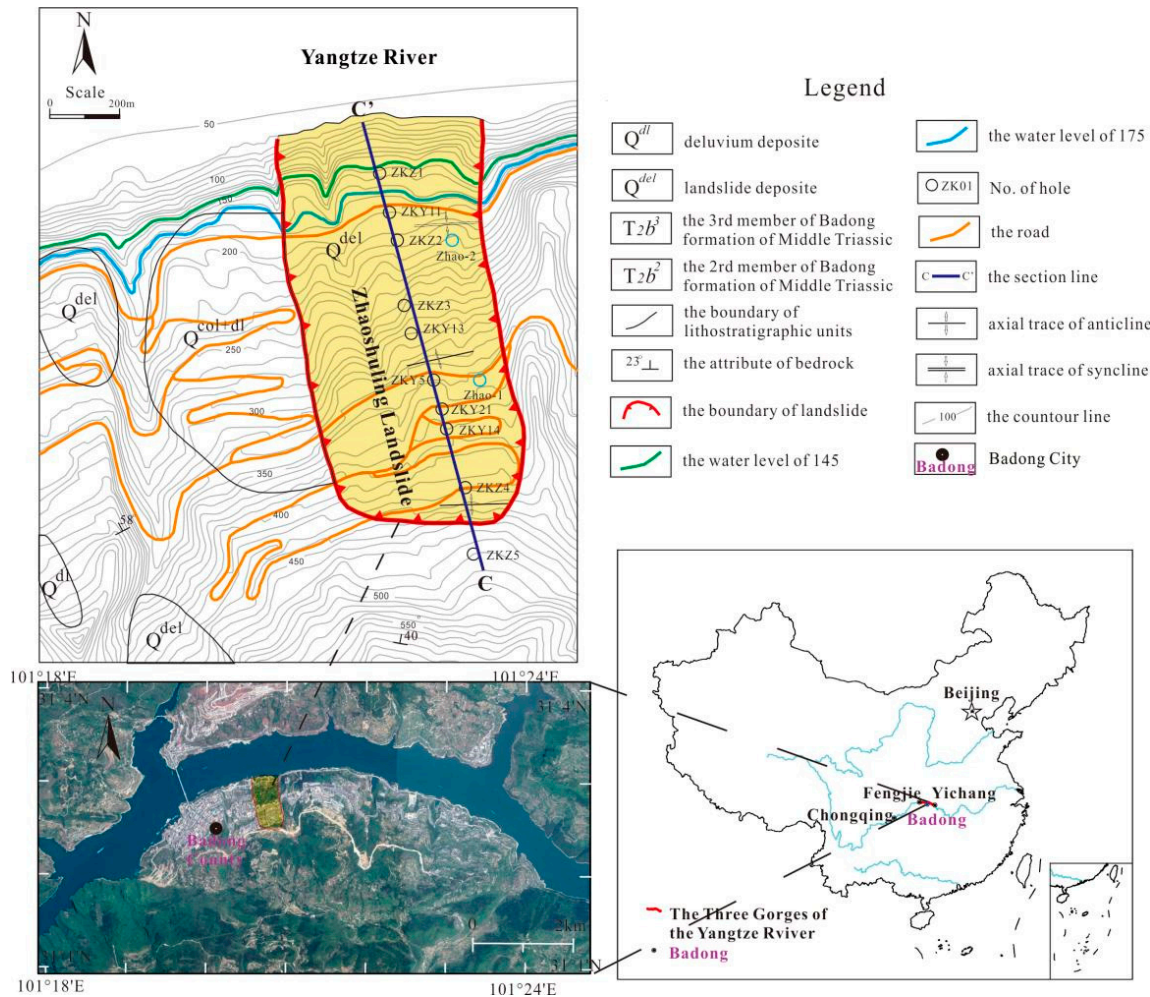


Figure 1. Engineering geological map of the Zhaoshuling Landslide.

However, the majority of the previous studies have focused on the inducing factors, which may only provide limited information regarding the complicity of the phenomena. However, the internal controlling factors, particularly the characteristics of the bedrock surfaces, are known to be the most important factors impacting the stability of landslide prone areas. This study found that the available technical reports backed up the theories that the different positions and shapes of the bedrock surfaces will lead to different deformation mechanisms of the landslides, along with the magnitude and distribution of pore pressure and stress in sliding bodies [13,17–20]. Therefore, considering the various types of reservoir landslides, integrated models of rainfall and water level variation conditions, bedrock surface shapes, internal action mechanisms, and the stability levels of landslide deformations with reservoir water level changes over time should be further investigated.

Various physical model experiments have been conducted under laboratory conditions, and the experimental results have been extensively applied to explore the features, stability, and evolution of landslides. Such investigations have provided improved insight into the failure modes and mechanisms related to the changes of different factors [21–24]. Subsequently, the similarities between the laboratory results and field observations were in-

investigated using the law of similitude, which has been employed extensively to investigate the fundamental principles of landslide movements [25–27].

In the present study, physical modeling was performed in order to examine the effects of chair-shaped bedrock surfaces on the reactivation of an ancient landslide under rainfall and reservoir water fluctuation conditions. The Zhaoshuling Landslide of Badong County was selected as the target of an interest. The pore water pressure, total soil pressure, and the landslide processes were obtained using experimental processes by analyzing the monitoring data of multiple systems. The obtained results improved the current understanding regarding the deformation characteristics and failure mechanisms of ancient landslides with chair-shaped bedrock surfaces under the conditions of rainfall and reservoir water fluctuations. The findings of this study provide an important basis for the prevention and mitigation of landslides in the reservoir areas.

## 2. Engineering Geology of the Zhaoshuling Landslide

Badong Town is a new residential area for immigrants in the Three Gorges Reservoir Region. It is located on the southern side of the Yangtze River. Many giant ancient landslide sites are located in this area, including the Zhaoshuling Landslide investigated in this study (as shown in Figure 1). The Zhaoshuling Landslide was characterized by a long strip shape and occurred on the right bank of the Yangtze River, approximately 6 km west of Badong County (as shown in Figure 2). Several deformation monitoring and stability analyses have been performed during the last several years for the purpose of studying the development of landslide deformations [28–35]. It was determined that based on the engineering geological survey results, the landslide's front has an elevation of 60 m and is submerged under the Yangtze River. In addition, the landslide's rear area has an elevation of approximately 460 m, and the two lateral sides are seated on a gully and a local fault, respectively. The landslide's length is 1260 m and its width had been determined to be 570 m. The total planar area measures  $61.2 \times 10^4 \text{ m}^2$ . Furthermore, based on the buried depths of the slide area revealed by drilled boreholes, along with the planar distribution of the landslide, it has been confirmed that the Zhaoshuling Landslide's volume was approximately  $3600 \times 10^4 \text{ m}^3$ .



**Figure 2.** Landscape details of the Zhaoshuling Landslide. (a) Satellite image of Zhaoshuling landslide (17 May 2017, from Google Earth); (b) Zhaoshuling landslide photograph (16 November 2016).

The landslide event was in the shape of a broken line with a slope angle varying between  $25^\circ$  and  $40^\circ$ . Three gently sloped platforms with elevations of 150 to 200 m, 350

to 425 m, and 475 to 500 m, respectively, can be observed along the longitudinal direction. Figure 1 provides a landscape photograph of the Zhaoshuling Landslide area, as well as the locations of exploratory boreholes. The highest platform is located at the rear of the landslide area with a slope angle of  $10^\circ$  to  $15^\circ$ . The lower platform is located in the front of the landslide with a slope angle of  $10^\circ$  to  $20^\circ$ . Figures 2 and 3 present the plan and sectional views of the Zhaoshuling Landslide engineering geological conditions, respectively.

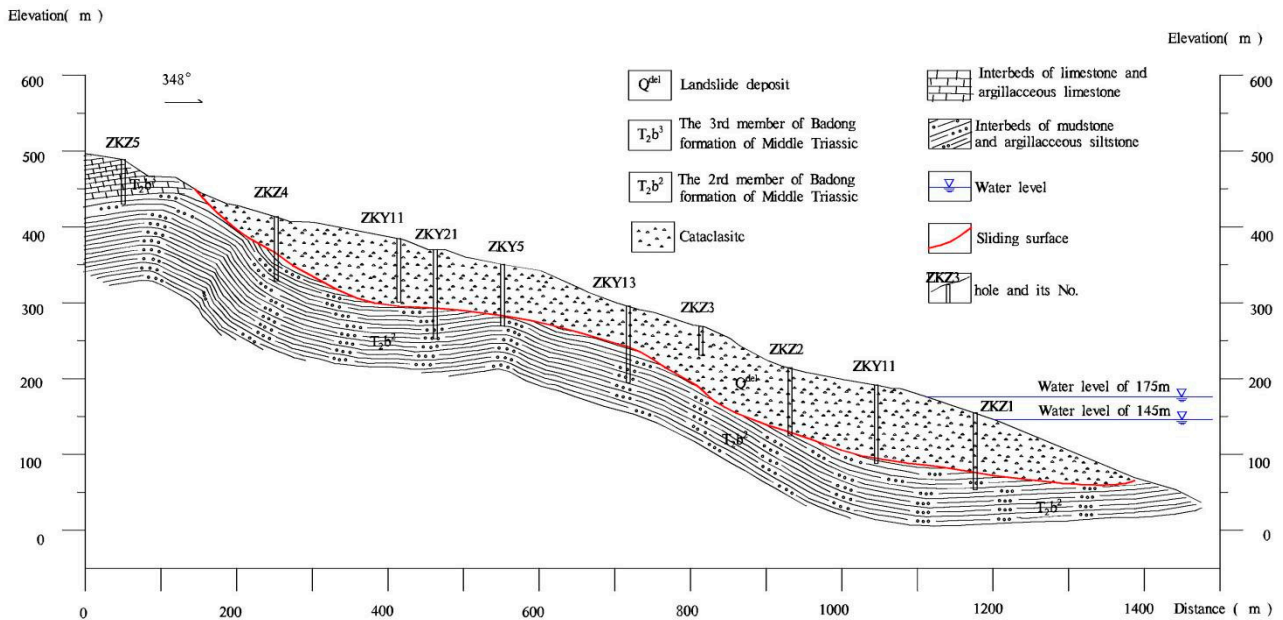


**Figure 3.** Engineering geological cross-section of the Zhaoshuling Landslide (C-C').

The structural features in the study area were found to be characterized by an E–W trending of multiple folds, as well as a series of reverse faults. The major feature among the fold structures was the Guandukou Syncline, in which the fold axis was observed to strike in a nearly E–W direction and axial trace extended along the southern bank of the Yangtze River. The syncline had manifested as an iso-thick symmetrical fold in the section. In addition, many asymmetrical secondary interlayer folds existed on the two flanks of the syncline, which were found to be mainly developed in the soft formations of the  $T_2b^3$  strata. In regard to the E–W trending reversed faults, the bedding faults or bedding shear zones were observed to be developed following a pattern of E–W folds due to extensive deformational forces. Additionally, along with the above-mentioned fault features, there were also well-developed conjugate joint systems, fracture zones, and various joints observed, as well as many other structural indications, such as gravitational creep-slippage and so on.

The Zhaoshuling Landslide moves along the interfaces of the  $T_2b^2$  and  $T_2b^3$  strata. The material of the sliding mass mainly consists of  $T_2b^3$  strata, with small amounts from the  $T_2b^2$  strata, and can be divided into two layers. The surface layer is mainly a khaki-brown soil-rock mixture, and subsurface mainly consists of quaternary landslide accumulation cataclastic rock masses, with most found to have retained the sequences of the original rock with layered structures. The lithologic characteristics of the bedrock have been determined to consist mainly of  $T_2b^2$  strata with purplish-red interbedded fine-grained argillaceous siltstone and silty mudstone. The sliding surface has been found to be composed of khaki disintegrated rock and gravelly clay, generally with thicknesses ranging between 0.3 and 0.5 m. The surface can be observed to be chair-shaped and is basically consistent with the relief of the local terrain.

As indicated by the results of previous studies, the slope composed of  $T_2b^3$  had easily become deformed as a result of the valley cutting and softening processes of the groundwater and reservoir water. Those progressive deformations generally developed

during multi-stages. The field investigation results indicated that no displacements had occurred when the reservoir's water levels were in the elevation range of 145 to 175 m each year. However, the deep sliding mass was prone to failure if the slide masses with  $T_2b^3$  strata were destroyed due to the lowering of reservoir water levels. Therefore, the interfaces of the  $T_2b^2$  and  $T_2b^3$  strata are considered to have been the major components of the Zhaoshuling Landslide, and their failure mechanism and processes were explored in this study. In order to simplify this study's model, the deep  $T_2b^2$  strata were treated as a slide bed.

### 3. Experimental Apparatus and Methodology

#### 3.1. Details of the Adopted Apparatus and Instrumentation

In the present study, a large gravity model test system was constructed, as shown in Figure 4. The test system was manufactured and operated by the China Three Gorges University, Key Laboratory of Geological Hazards on Three Gorges Reservoir Area, and the Ministry of Education, Yichang, China. The test system consisted of a hydraulic control lifting system; reservoir water level control system; fixed-head water supply and drainage system; artificial rainfall system; and an observation and data acquisition system, as detailed in Figure 5.



Figure 4. Landslide model test system.

The model box size measured 8.0 m (length)  $\times$  0.8 m (width)  $\times$  3.5 m (height). The sidewalls were smooth and transparent so that the deformations could be observed and recorded from either side of the model box. In addition, the base and side walls of the model box were reinforced with steel sections. The lifting system included hydraulic pressure jacks connected to the base of the model box. The maximum specified slope angle of the model box to the horizontal was 20°.

The main purposes of this study's model tests were to solve the following questions:

1. How could the Zhaoshuling Landslide event have been triggered as the result of the rise and fall in rainfall and reservoir water levels, causing deformations and failure to

occur; and 2. Whether or not the deformations and failure of the upper sliding body had been affected by the undulating state of the lower sliding surface. It was believed that the answers to the aforementioned questions could be achieved using the monitoring and observational data of the displacements and pore water pressure levels at various locations in this study’s model during different time periods.

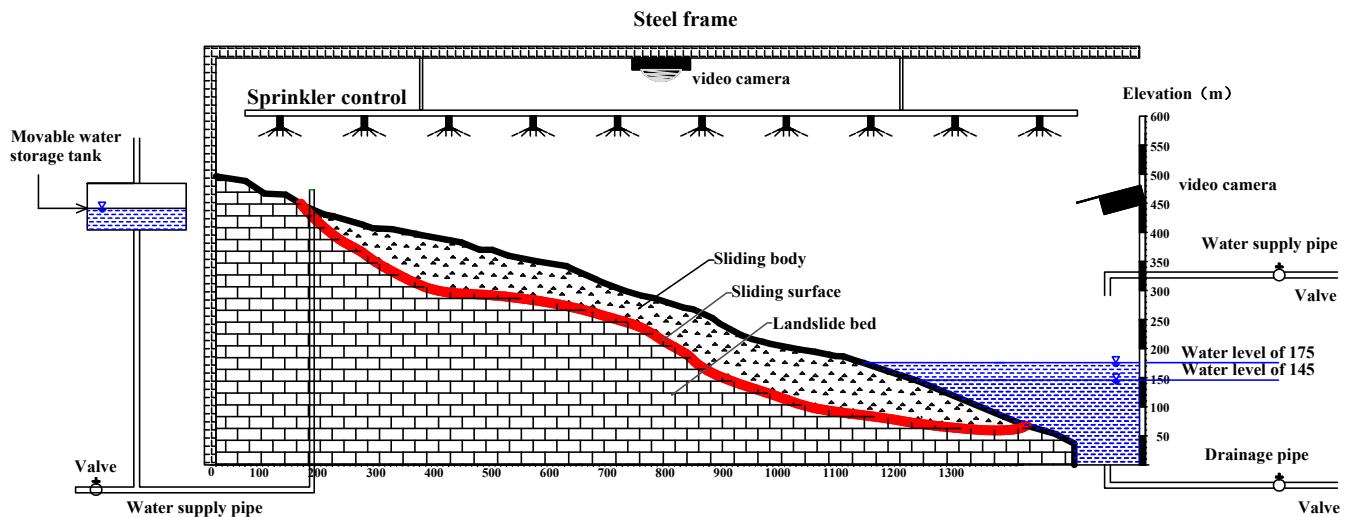


Figure 5. Geological simplified model of the Zhaoshuling Landslide event.

### 3.2. Law of Similitude

In the present research investigation, considering the size limitations of the model box, the physical experiments were generally scaled down. The physical parameters in the prototype-scale could be correlated with those in the model-scale using the similitude ratios, detailed as follows:

$$C_q = q_p / q_m \tag{1}$$

where  $C_q$  represents the the similitude ratio;  $q$  indicates the corresponding parameter; and the subscripts  $p$  and  $m$  denote the prototype and the model, respectively.

During the modeling processes, the parameters involved the dimension  $l$ ; density  $\rho$ ; acceleration of gravity  $g$ ; cohesion  $c$ ; internal friction angle  $\phi$ ; Young’s Modulus  $E$ ; Poisson’s Ratio  $\mu$ ; stress  $\sigma$ ; strain  $\varepsilon$ ; displacement  $u$ ; permeability coefficient  $k$ ; time  $t$ ; velocity  $v$ ; suction  $s$ ; moisture content  $\theta$ ; rainfall intensity  $q$ ; and lateral pressure  $p$ . Therefore, following the  $\pi$ -Theorem, all of the aforementioned parameters that correlated with the landslide must meet the following equation:

$$F(l, \rho, g, c, \phi, E, \mu, \sigma, \varepsilon, u, k, t, v, s, \theta, q, p) = 0 \tag{2}$$

where  $\phi, \mu, \varepsilon, \theta$  are the non-dimensional parameters. If the equation was complete, its solution had a form with chosen numbers of independent scaling products ( $\pi$ -terms). Therefore, by choosing  $l, g, \rho$  as the independent parameters, Equation (1) could be re-written in terms of those three non-dimensional scaling parameters as follows:

$$F(\pi_1, \pi_2, \pi_3) = 0 \tag{3}$$

where

$$\begin{aligned} \pi_1 &= \frac{c}{l\rho} \\ \pi_2 &= \frac{k}{(lg)^{1/2}} \\ \pi_3 &= \frac{t}{(l)^{1/2}(g)^{-1/2}} \end{aligned} \tag{4}$$

Then, if the similitude ratios of  $C_\phi$ ,  $C_\rho$ , and  $C_g$  are set equivalent to unity, the similitude ratios of  $C_l$ ,  $C_c$ ,  $C_\sigma$ , and  $C_p$  are assigned as  $n$ , the other scaling parameters can be easily derived as follows:

$$\begin{aligned} C_\rho &= C_g = C_\phi = C_\mu = C_\varepsilon = 1 \\ C_l &= C_u = C_c = C_E = C_\sigma = C_p = n \\ C_k &= C_v = C_q = C_t = \sqrt{n} \end{aligned} \quad (5)$$

In the current study, the Zhaoshuling Landslide was simplified into a 2D model for the model testing process. The size of the model was scaled down to 1/400 of the full scale of the Zhaoshuling Landslide due to the limitations of the model box.

### 3.3. Physical Parameters of the Model's Similar Materials

The model testing processes were required to reproduce the characteristics of the prototype slope, particularly for such progressive failures as the overall shear failure. The main issue was to simulate the deformation mechanism with similar materials.

In this study, normal sand, barite powder, iron powder, glycerin, bentonite, and ordinary Portland cement were used for the mixing of the similar materials. Among those, the barite powder and iron powder were used to improve the apparent density. Then, glycerol and bentonite were added binders. Ordinary Portland cement was used to improve the water resistance of the similar materials. The slide bed was simulated using barite powder, cement, and gypsum, along with water. The slip soil was composed of polyvinyl chloride film material.

The physical and mechanical parameters of prototype slip slope were obtained from the physical and mechanical tests. The parameters of the model slip mass were obtained from the similarity theory, then the materials were created by means of the mix proportion tests. Direct shear tests between the slide bed and the geomembrane were also conducted in the laboratory to test the ability of these interfaces to simulate the slip soil. The results show that the test parameters under the final ratio can meet the needs of actual landslide model test. The physical and mechanical properties of the similar materials used in the model tests are presented in Table 1.

**Table 1.** Comparison between the prototype material parameters and the model material parameters.

Parameter	Slip Mass		Slip Band	
	Prototype	Model	Prototype	Model
Bulk density (g/cm <sup>3</sup> )	2.6 to 2.7	2.6	-	-
Young's modulus (MPa)	1200 to 2560	5.2	-	-
Poisson's Ratio	0.28 to 0.31	0.30	-	-
Cohesion (KPa)	2 to 12.2	0.02	15	0.038
Internal friction angle (°)	32 to 35	32	30	30

### 3.4. Test Plan for the Large-Scaled Model Testing Processes

The slope profile and interface locations were determined prior to the backfilling by drawing the slope model contours on the glass model box. Then, prior to placing the soil sample into the simulation box, the glass walls were lubricated in order to reduce the frictional effects of the sidewalls. After laying and fixing the PVC film on the sliding bed, the mixed materials were placed in the simulation box and compacted for every 2 cm of lift in order to achieve the target density. Then, after the compaction process was completed, the slope was cut according to the contour line.

Throughout this study's testing procedures, displacement meters, pore pressure sensors and soil pressure sensors were set into the large-scaled models, as presented in Figure 6. The details of the instrumentations are summarized in Table 2. All of the sensors were placed uniformly in the toe, middle, and rear zones. However, due to the small thickness of the sliding body in this study's model tests, the sensors were all arranged on the sliding surface, and the sensors in the same section were arranged in the same row. In addition, in

order to record the effects of the sliding surface geometry on the propagation of the landslide, one group of sensors (No. 2) was positioned on the concave part of the chair-shaped surface. Each instrument was calibrated prior to installation. All of the instruments inside the slope model were installed during the placement of the mixed materials. Furthermore, all of the electrical instruments were connected to a data-logger for the convenience of automatic data recording, and each of the entire testing processes were video-taped. Figure 7 illustrates the construction of the physical simulation models.

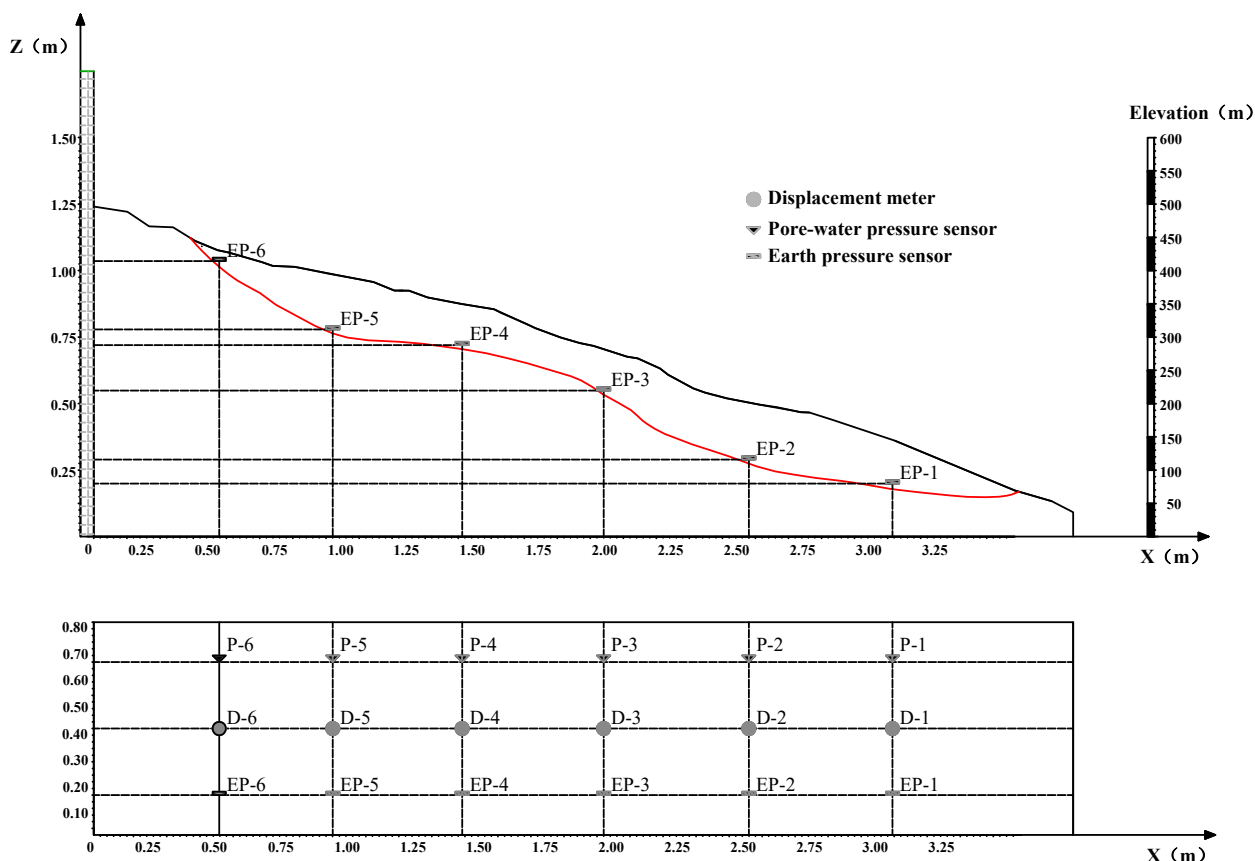


Figure 6. Monitoring layout of the test models.

Table 2. Instrumentation installed in the slope model.

Type of Instrument	Measurement	Quantity	Measuring Range
Resistance strain pore water pressure sensor	Pore water pressure	6	0 to 50 kPa
Resistance strain soil pressure sensor	Soil pressure	6	0 to 50 kPa
Resistive displacement meter	Displacement	6	<100 mm
Flowmeter	Flux	1	16 to 160 mL/min

In view of the set goals of this study’s experiments, two model tests were conducted using different experimental processes. The testing procedures are listed in Table 3. In accordance with the Three Gorges Reservoir operating program, the reservoir water levels were known to fluctuate between 145 m and 175 m. Additionally, considering the similarity relationship, the rise and fall in the water level were determined to be 4.2 mm/h, which corresponded to a real speed of 2.0 m/d. Therefore, it was believed that the experimental processes could accurately and realistically reflect the actual conditions.



**Figure 7.** Construction of the physical simulation models: (a) Slide bed; (b) Slide surface; (c) Slide mass; (d) Entire model.

**Table 3.** Testing procedures for the models.

Slope	Test Objective	Procedure
Model 1: Natural slope	To simulate landslide deformations and failure occurring with water level fluctuations	<p>(1) A flow control device was used to control the flow into the reservoir from the initial level at an elevation of 36.25 cm (corresponding to 145 m of real elevation) to the normal level at an elevation of 43.75 cm (corresponding to 175 m of real elevation) during an 18 h time period. The reservoir water level was maintained at 175 m for 1 h.</p> <p>(2) The water level control valve was opened in order to discharge water from the reservoir. Then, the water level outside the slope model was decreased from a 43.75 cm elevation to a 36.25 cm elevation within an 18 h period. Finally, the water level of the reservoir at that elevation was maintained.</p>
Model 2: Natural slope	To simulate the coupling effects of water level fluctuations and rainfall on the landslide event	<p>(1) A flow control device was used to control the flow into the reservoir from the initial level at an elevation of 36.25 cm to the normal level at an elevation of 43.75 cm during an 18 h period. The reservoir water level was maintained at 175 m for 1 h.</p> <p>(2) When the water level control valve was opened, a sprinkler device began operation at the same time, which simulated a rainstorm with a rainfall intensity of 0.42 mm/h (corresponding to 200 mm/d of real intensity). The control duration was set as 3.6 h (corresponding to 3 days of real time). The water level drop rate was the same as that of Model 1, and finally the reservoir water level was maintained at 145 m.</p>

#### 4. Test Results and Observations

##### 4.1. Pore Water Pressure and Soil Pressure Responses to Rises in Water Levels

The pore water pressure levels measured in this study by the six piezometers are shown in Figure 8. The piezometers (labelled P-1, P-2, P-3, P-4, P-5, and P-6) were installed at the elevations of 0.2 m (80 m), 0.3 m (120 m), 0.55 m (220 m), 0.725 m (290 m), 0.775 m (310 m), and 1.025 m (410 m), respectively. It was observed that the pore water pressure levels measured by the piezometers at the different elevations displayed different results with time in response to the changes in the water levels.

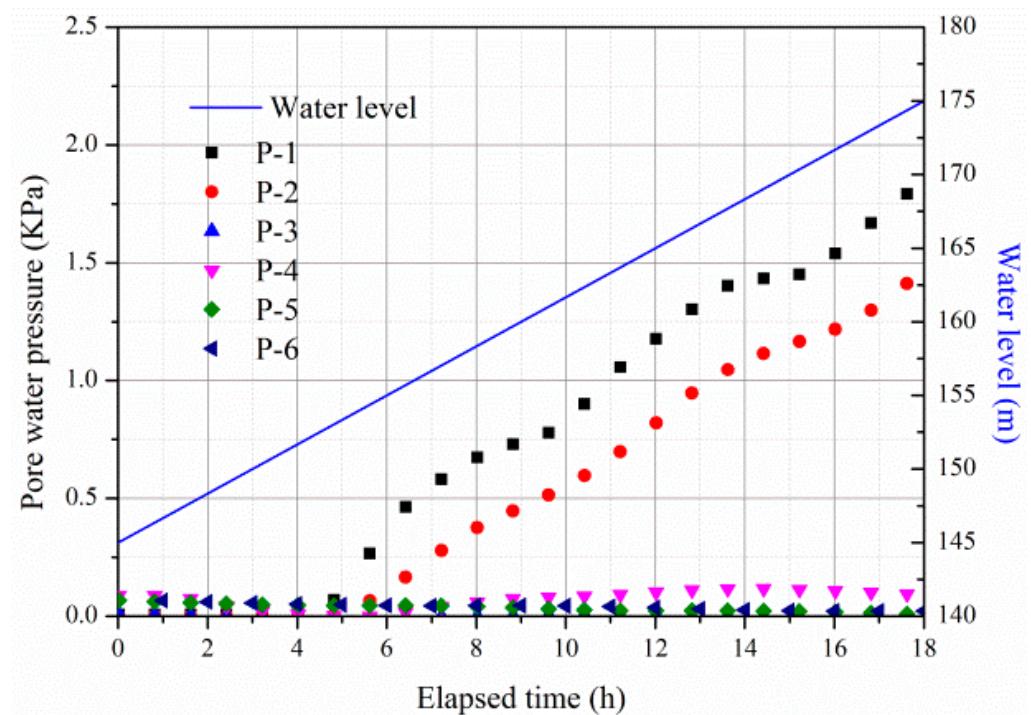


**Figure 8.** Pore water pressures during the rises in the water levels.

At the beginning of the experimental process, it was observed that all of the pore water pressure sensors had displayed no responses to the rising water levels when the valve was switched on, allowing the water flow into the slope. However, when the reservoir water level had risen to 38.13 cm (corresponding to 152.5 m of real elevation), the P-1 piezometer had displayed a response. Following that, the P-2 piezometer located at an elevation of 30 cm was observed to respond to the reservoir water level changes at approximately five hours after the start of the experiment. However, there were no changes during the rising of the reservoir water levels according to the measurement results of the P-3, P-4, P-5, and P-6 piezometers located in the middle and rear areas of the landslide site. The pore water pressure levels of the P-1 and P-2 piezometers were confirmed to have increased linearly with the rising of the reservoir water levels.

Figure 9 shows the total stress values measured by the six soil pressure sensors installed in the slope model. The changes in total soil pressure levels were in response to the rising water levels. In addition, the slope seemed to have become more uniform as the water levels on the slope rose. Moreover, the total soil pressure seems to have been influenced by the water pressure levels, since the total soil pressure also increased with the rising water levels.

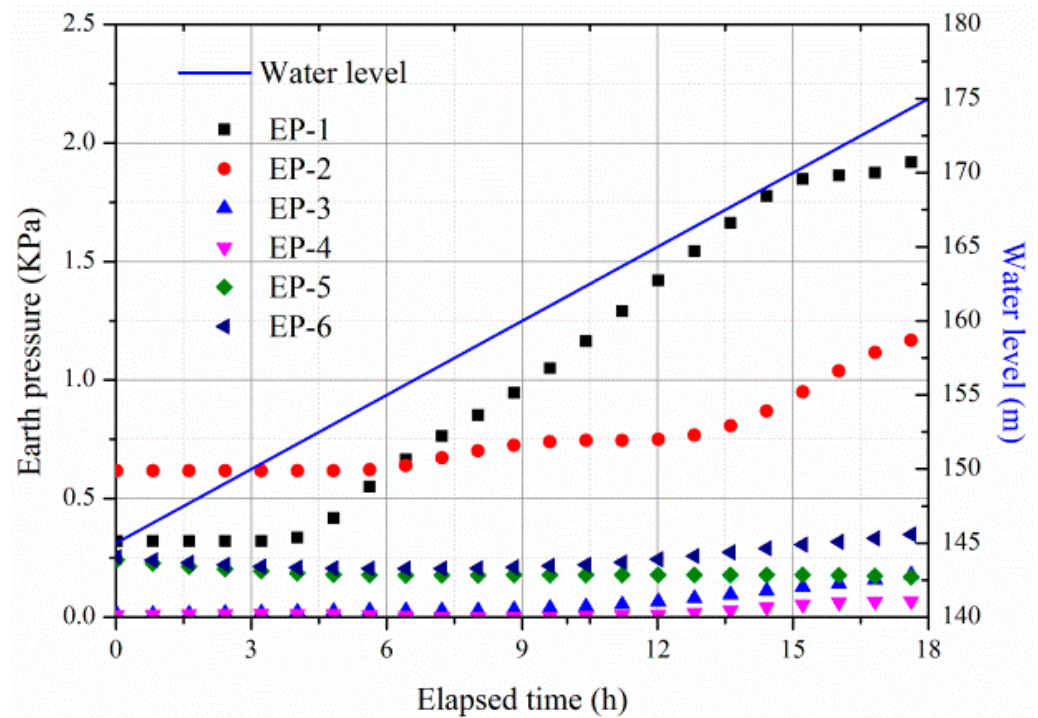


**Figure 9.** Soil pressure levels during the rises in the water levels.

The soil pressure sensors EP-1 and EP-2 presented a similar general trend during the increase in water levels. For example, the total stress recorded by the EP-1 sensor increased from an initial value of 0.32 kPa to a final value of 1.94 kPa. Additionally, there was an incremental change of 1.62 kPa observed within 18 h following the commencement of this study's experiment. The total stress recorded by the EP-2 sensor increased from an initial value of 0.62 kPa to a final value of 1.18 kPa, with an incremental change of 0.56 kPa observed as the water level rose within the aforementioned 18 h period. However, the total stress recorded by the Ep-3, Ep-4, EP-5, and EP-6 sensors, which were located in the middle and rear zones of the slope model, were not found to change.

#### 4.2. Pore Water and Soil Pressure Level Changes in Response to the Lowering of the Water Levels

Figure 10 details the pore water pressure responses with the water level changes recorded by the piezometers at different elevations. It can be seen in the figure that the pore water pressure levels of the P-1 and P-2 piezometers at the elevations of 0.2 m (80 m) and 0.3 m (120 m), respectively, showed a similar general trend during the lowering of the water levels. Furthermore, there was a small delay observed in the pore water pressure relative to the lowered water levels of the model slope. When the water levels of the slope were lowered by 0.075 m, the pore water pressure recorded by the P-1 and P-2 piezometers had decreased by 1.77 kPa and 1.18 kPa, respectively. However, it was found that the pore water pressure levels recorded by the other sensors located at the middle and rear zones of the slopes had displayed little change.

Figure 11 presents the results of the soil pressure levels measured by the six soil pressure sensors in response to the lowering water levels. The total stress of the soil pressure of the EP-1 sensor, which was located at 0.2 m in the slope, decreased from an initial value of 1.94 kPa to 0.17 kPa. In regard to the EP-2 soil pressure sensor, which was located higher than the EP-1 sensor, it was observed that the pressure had decreased from an initial value of 1.18 kPa to 0.07 kPa. Therefore, the decreasing trend of the total stress was found to be the same as that of the pore water pressure.

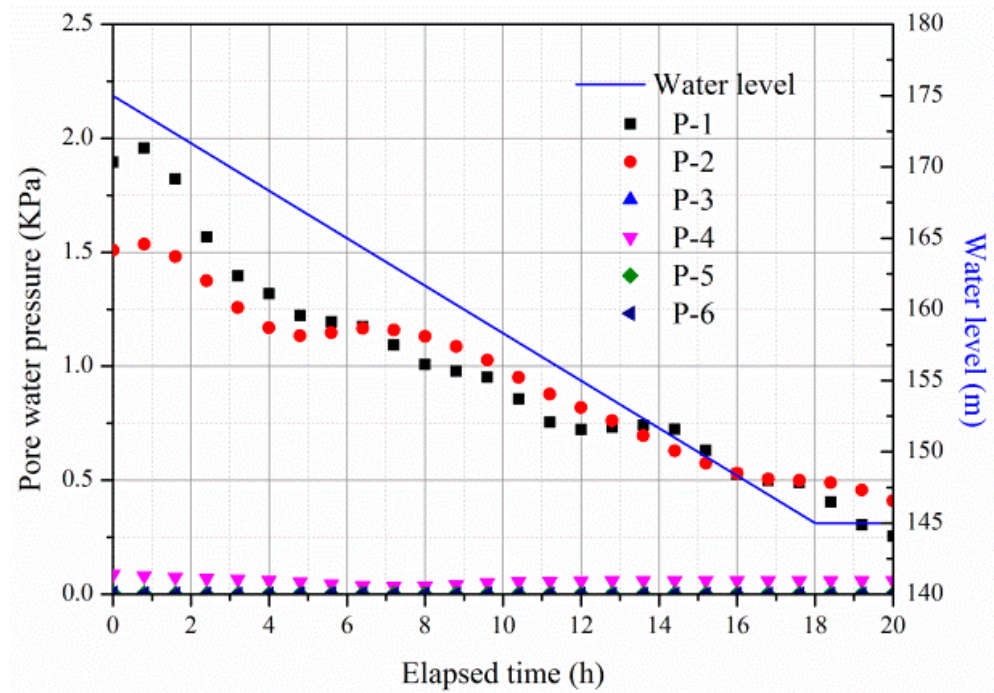


Figure 10. Pore water pressure levels during the water level lowering process.

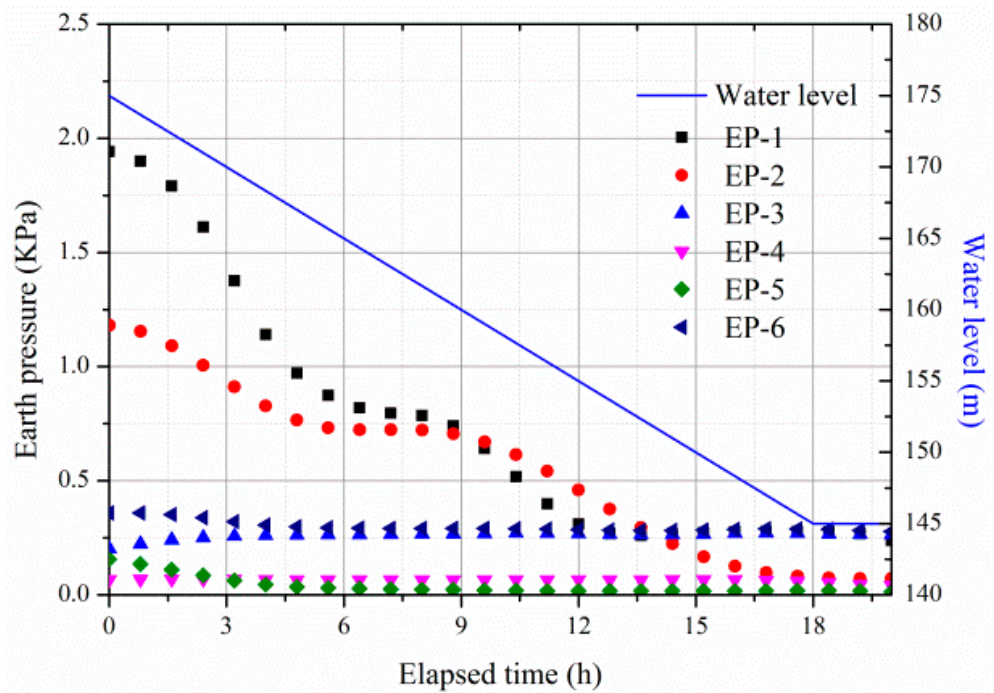
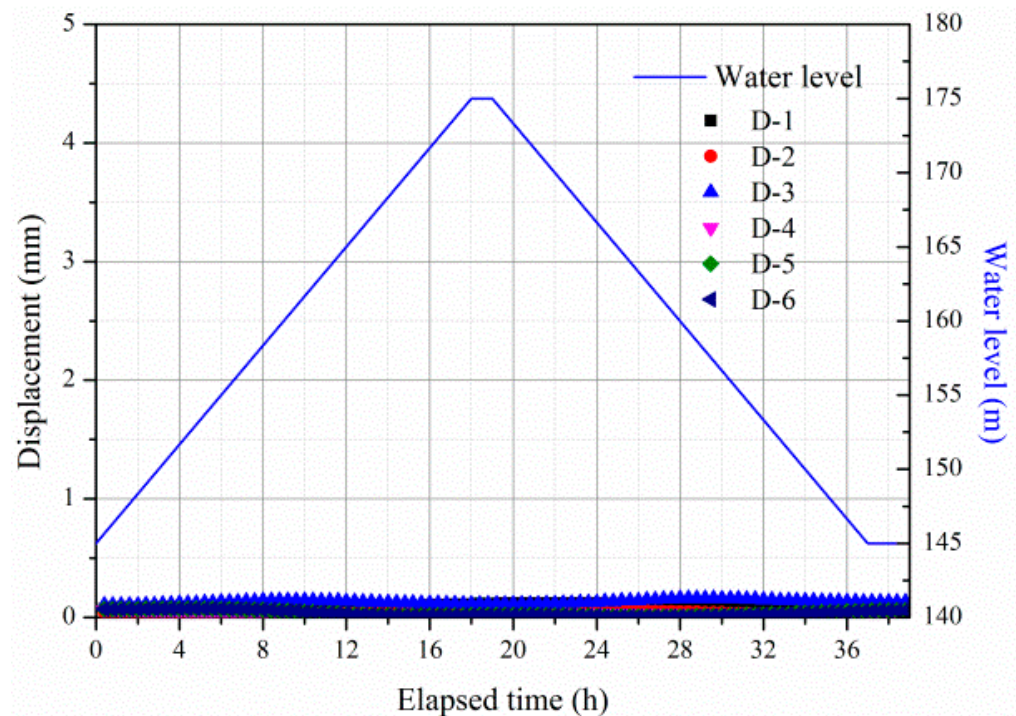


Figure 11. Soil pressure during the water level lowering process.

In summary, by referring to measurement results of the different displacement sensors, no deformations were observed to have occurred during the aforementioned processes of this study’s model, and no cracks had been observed on the slide surface, as shown in Figure 12.



**Figure 12.** Displacements observed during the rising and lowering of the water levels.

#### 4.3. Responses of the Slope Model during the Water Level Lowering Process Combined with the Rainfall Process

##### 4.3.1. Visual Observations during the Processes

In order to simulate the coupling effects of the water level fluctuations and rainfall events on the investigated landslide, another identical model was constructed. Similar to the first model, the same rising and lowering of the reservoir water levels were conducted in the second model during the reservoir impounding and water level lowering processes. When the water level lowering rate was approximately 4.2 mm/h, a rainfall simulation device was activated. The rainfall occurred with an intensity of 0.42 mm/h, which was similar to the rainfall intensity (200 mm/d) of the prototype. The rainfall duration time was controlled as 3.6 h, which corresponded to three days of real time.

A video camera was mounted in front of the slope in order to record the failure initiation and subsequent movements during the water level lowering processes. The slope profiles associated with the displacements before and after failure were also recorded. The failure process of the slope model is systematically shown in Figure 13a–c, respectively. The failure mechanism observed and documented in this study's large-scaled slope model experiment was apparently complex, and the following phenomena were observed during the water level lowering and rainfall simulation processes.

The lowering water level, combined with heavy rainfall, was observed to initiate the formations of a transverse tension crack in the middle of the slope model. The crack occurred in the middle of the slide mass at approximately the 30 min point following the commencement of the water lowering and rainfall simulations, as shown in Figure 13a.

The length and breadth of the tension crack increased with the lowering water levels combined with the rainfall simulations. The length of the tension crack increased as the water levels reached the lower parts of the slopes, as illustrated in Figure 13b,c. Then, obvious sliding deformations were found to have immediately occurred in the middle and toe sections of the slope model. The entire deformation zone of the slope model was bounded at an elevation of approximately 300 m. However, the slope material behind the deformation zone appeared to remain stable. As can be seen in the figures, the obvious deformation region during the model tests was located in the lower zone at an elevation of approximately 300 m.

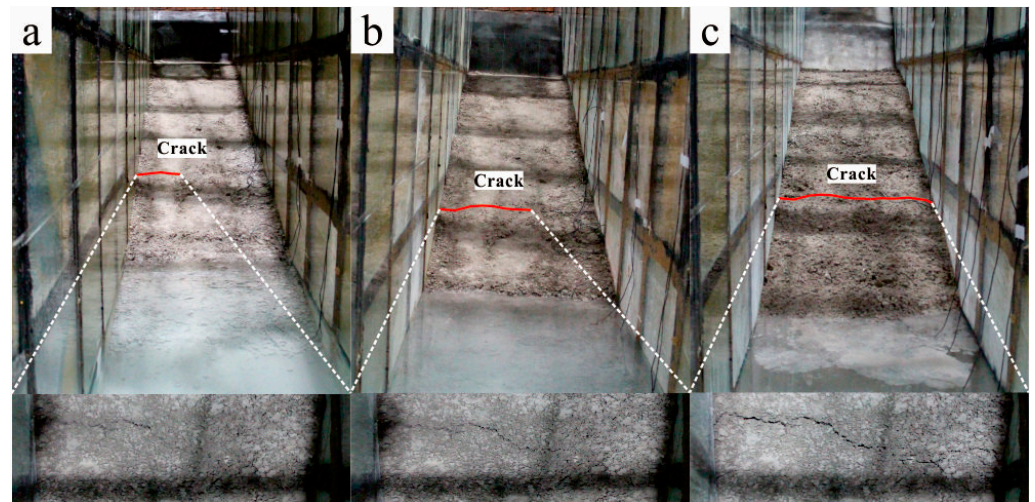


**Figure 13.** Water lowering processes combined with rainfall simulations of the induced landslide process: (a) Cracking occurred in the middle of the landslide with a water elevation of 43.54 cm; (b) Crack propagation with a water elevation of 41.25 cm; (c) Crack penetration with a water elevation of 40.18 cm.

The displacement data shown in Figure 14 are expressed in millimeters. It should be mentioned that due to sensor failure, sensor readings were not collected by the D-1 and D-6 sensors, and no further results are shown in Figure 14. However, based on the monitoring data recorded by the other four displacement sensors, the deformations were found to be small in the areas of the D-3, D-4, and D-5 sensors, which were located in the middle and rear sections of the model, during the entire experimental process, whereas the deformations at the toe had increased sharply to 14 mm following the rainfall simulations, as shown in Figure 14.

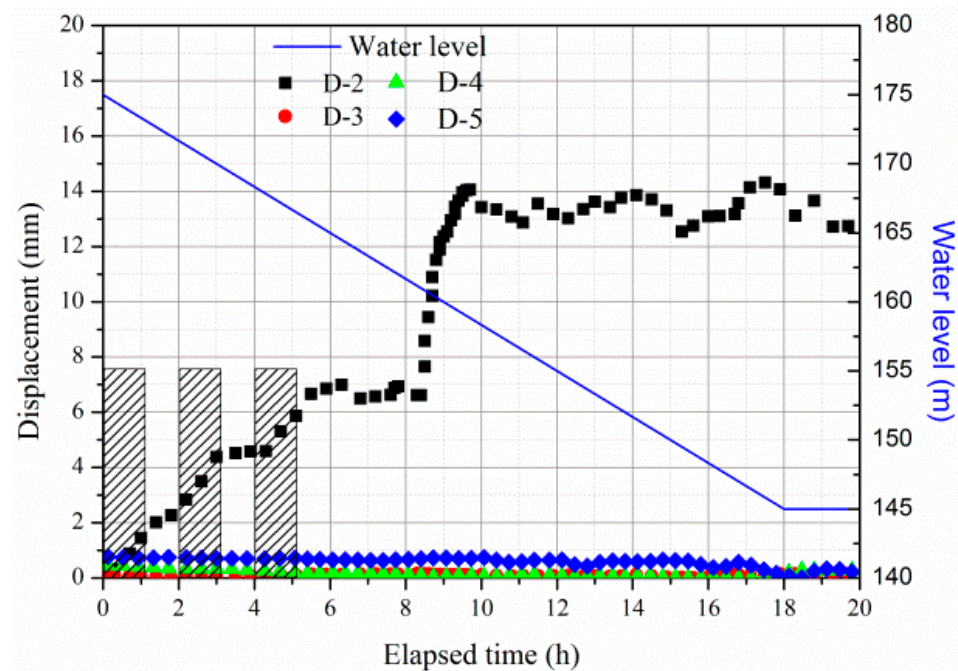


**Figure 14.** Displacements observed during the water lowering process combined with the rainfall simulations.

#### 4.3.2. Pore Water and Soil Pressure Levels during the Experimental Processes

Figure 15 presents the pore water pressure levels measured by the six pore pressure gauges mounted in the slope model. The changes in pore water pressure were in response to lowering of the water levels combined with the rainfall simulations. The variations in the pore water pressure levels were divided into three types.

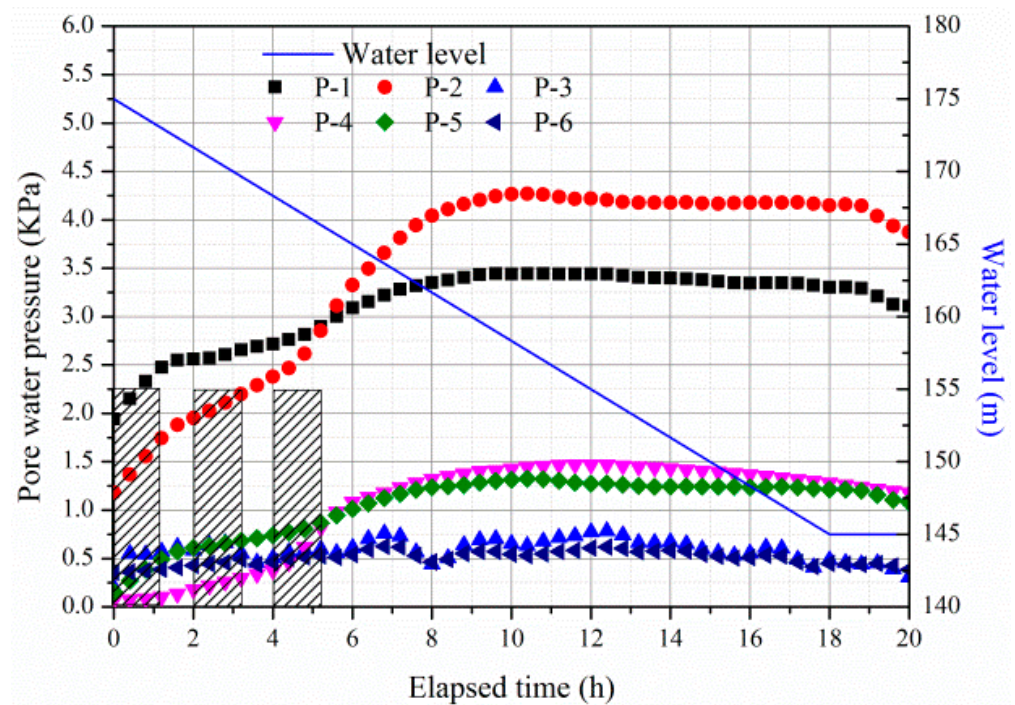


**Figure 15.** Pore water pressure levels recorded during the water lowering process and rainfall simulations.

The pore water pressure levels recorded by the P-1, P-4, and P-5 piezometers were observed to have gradually increased from initial pore water pressure levels of 1.94 kPa, 0.07 kPa, and 0.16 kPa to 3.44 kPa, 1.47 kPa, and 1.33 kPa, respectively. The incremental changes of 1.50 kPa, 1.40 kPa, and 1.17 kPa occurred within an 18 h timeframe after the initiation of the experiment. The pore water pressure levels recorded by the P-3 and P-6 piezometers were found to have changed little during the entire experimental process, with increases from initial total stress levels of 0.20 kPa and 0.36 kPa to 0.78 kPa and 0.63 kPa, respectively. The incremental changes of 0.58 kPa and 0.27 kPa had occurred within 18 h following the initiation of the experiment. However, the pore water pressure levels recorded by the P-2 piezometer were found to have increased sharply from an initial total stress of 1.18 kPa to 4.27 kPa, an incremental change of 3.09 kPa.

Figure 16 details the soil pressure levels measured by the six soil pressure gauges installed in the slope model. The changes in soil pressure were also in response to lowering water levels combined with the rainfall simulations. The soil pressure levels measured by the P-1 and P-5 piezometers showed similar results within 18 h following the commencement of the experiment, with gradual increases observed from the initial pressure levels of 1.94 kPa and 0.16 kPa to 3.40 kPa and 1.14 kPa, respectively. The soil pressure levels measured by the P-3 and P-6 piezometers were found to display only minimal changes during the entire experimental process, with increases from initial soil pressure levels of 0.20 kPa and 0.36 kPa to 0.75 kPa and 0.63 kPa, respectively. The data range fluctuation characteristics which were recorded by the P-4 piezometer during the final 18 h displayed incremental changes of 0.80 kPa. However, the soil pressure levels recorded by P-2 piezometer were observed to increase sharply from an initial soil pressure of 1.18 kPa to 3.67 kPa. Therefore, an incremental change of 2.48 kPa had occurred.

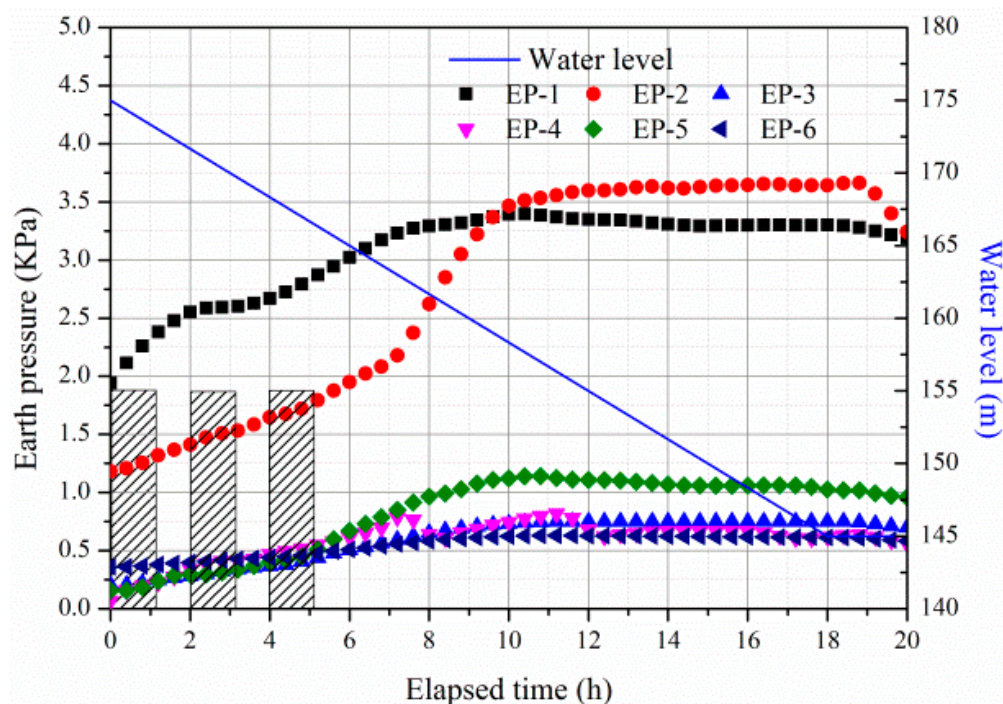


**Figure 16.** Soil pressure levels recorded during the water lowering process and rainfall simulations.

## 5. Discussion

### 5.1. Comparison of the Two Models

This study's comparison of Model-1 and Model-2 revealed the following:

- (1) The rise and fall of reservoir water levels had little effect on the middle and rear sections of the landslide site.
- (2) The landslide mass was stable during reservoir impoundment and discharge processes.
- (3) The displacements increased, and finally failure occurred when the water levels rapidly decreased, combined with the effects of rainfall.

It was observed that, differing from Model-1, the soil and pore pressure levels in all parts of Model-2 displayed a tendency to increase at first and then decrease following the simulated rainfall, as shown in Figures 15 and 16. It was determined that this was due to the fact that the rain had infiltrated into the slope through the pores and cracks of the landslide model, which resulted in increases in the pore water and soil pressure levels, as well as increased weight of the rock and soil. Then, after the rainfall had ceased, the groundwater inside the slope was discharged into the reservoir, resulting in decreased groundwater levels and gradual decreases in the pore water pressure. The rises in the soil pressure levels during the early part of the process also indicated stress concentrations and accumulations of strain energy in the slope. The maximum soil pressure was the result of the coupling of the reservoir water levels and the effects of rainfall. The continuous decreases in the soil pressure during the latter part of the process were determined to be due to the release of strain energy inside the slope and the redistribution of the stress following the deformations of the rock and soil masses within the landslide.

It can be seen in Figure 15 that during the lowering of the water level combined with the rainfall process, the data of the pore water pressure recorded by P-2 piezometer (located at the toe of the landslide) had increased rapidly. In addition, the rising rate of the pore water pressure was higher than that recorded by the sensors in other parts of the landslide site. The piezometers located above the bedrock and near the middle and rear zones of the slope showed pressure rises of between approximately 0.27 and 1.50 kPa following the rainfall simulations. However, the pore water pressure recorded by the piezometer installed at the toe of the slope showed an increase of 3.09 kPa in response to the same rainfall simulations.

### 5.2. Influences of the Chair-Shaped Bedrock Surface on the Groundwater Levels as per the Monitoring Data

Pore phreatic water is the main form of groundwater in the Zhaoshuling Landslide area. Its recharge occurs at the upper part of the landslide as a result of bedrock fissures and atmospheric precipitation, which eventually discharges into the Yangtze River following the infiltration of the landslide body. This was determined through the data of the borehole monitoring of the groundwater levels which had been performed in the main part of the landslide site. In order to study the influencing effects of chair-shaped surface on groundwater levels under the conditions of rainfall and reservoir water level changes in the Zhaoshuling Landslide area, the data from boreholes Zhao-1 and Zhao-2 located in different parts of the landslide site were selected for further analysis in this study. The borehole locations are also shown in Figure 2. The groundwater level monitoring processes at the Zhao-1 and Zhao-2 boreholes have been conducted since May of 2006, and the monitoring period ranged from May of 2006 to November of 2012.

Figure 17 shows the effects of the rainfall and reservoir water fluctuations on the changes in groundwater levels. Borehole Zhao-1 was located in the middle part of the landslide site and had a higher elevation and groundwater level than borehole Zhao-2, which was located at the toe of the landslide site. Therefore, the groundwater at the Zhao-1 borehole was less affected by the reservoir water levels than the Zhao-2 borehole. The changes in groundwater levels in the borehole were dominated by the rainfall effects. However, the amount of surface runoff was larger than that of the infiltration during rainfall events in that area, and the water level fluctuations at borehole Zhao-1 were observed to be small.

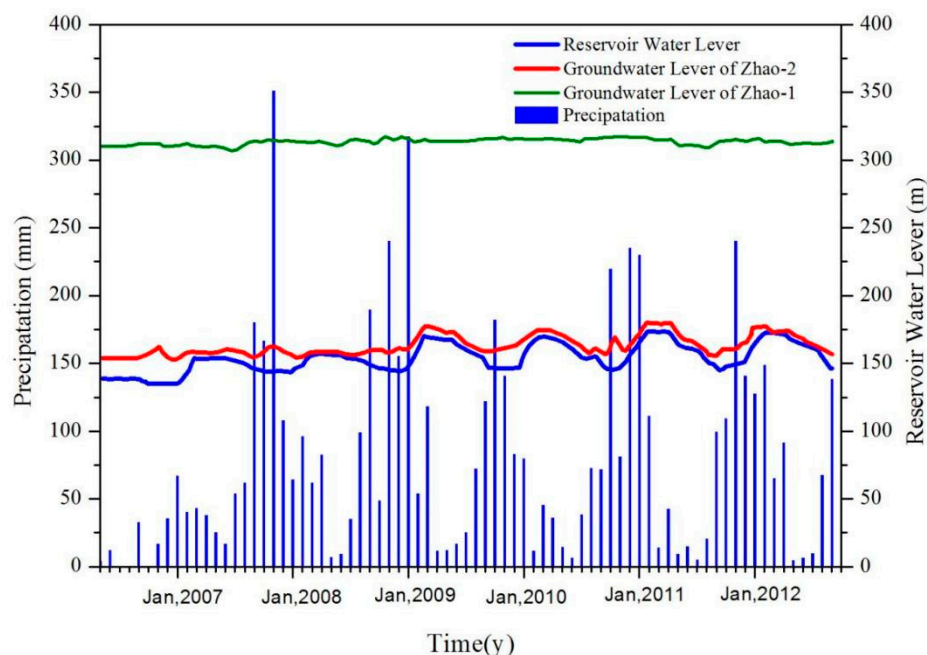


**Figure 17.** Relationships between precipitation, reservoir water levels, and groundwater levels of the Zhao-1 and Zhao-2 borehole sites.

Borehole Zhao-2 was located at the toe of the landslide site. During the period of the reservoir water fluctuations and the rainy seasons during the study period (May of 2006 to November of 2012), the changes in groundwater levels of the Zhao-2 corresponded to the variations in the rainfall and reservoir water levels. Figure 17 shows that the fluctuations in the groundwater levels were consistent with that of the reservoir water levels and had also lagged behind that of the reservoir water levels.

Figure 18 presents the effects of the rainfall on the changes in the rates of the groundwater levels. It was found that under the same precipitation conditions, the change rates

of the groundwater levels in the Zhao-2 borehole were greater than that of the Zhao-1 borehole during rainy seasons. These results indicated that the changes in the groundwater levels in the Zhao-2 borehole were more easily affected by rainfall than those of the Zhao-1 borehole. The test results were found to be in accordance with the monitoring data. The higher groundwater level changes in the Zhao-2 borehole, which was in the same position as P-2 in this study's model, indicated that poor drainage conditions existed.

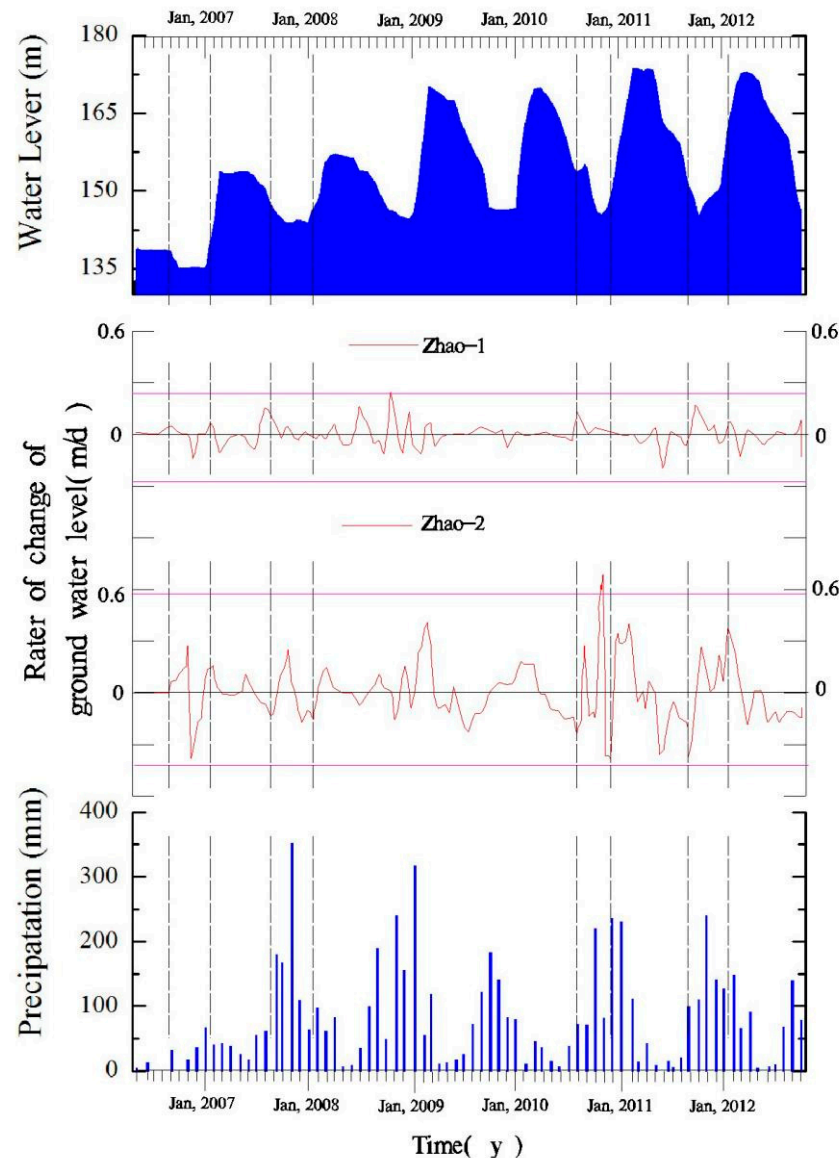


**Figure 18.** Relationships between the precipitation and the changes in the rates of the ground water levels in the Zhao-1 and Zhao-2 boreholes.

### 5.3. Conceptual Model of a Slope Failure with a Chair-Shaped Bedrock Surface

In the current research investigation, a striking feature was observed after examining the cross-sections of the landslide site. That is to say, the rockhead profile was found to be chair shaped. The Guandukou Syncline and Badong Fault were found to strike an E–W control of the tectonic framework and geomorphologic characteristics of the Zhaoshuling Landslide. The Guandukou Syncline was determined to be composed of multiple secondary folds, which are mainly asymmetric, and box folds forming a chair-shaped bedrock surface. The chair-shaped bedrock surface was observed to be generally parallel to the slope surface. However, at the toe of the slope, the interfaces become rather flat or slightly depressed, or even upside down. It was found that the chair-shaped bedrock formation at the toe of the

slope had significant adverse effects on the mechanisms of the slope stability, as detailed in Figure 19.

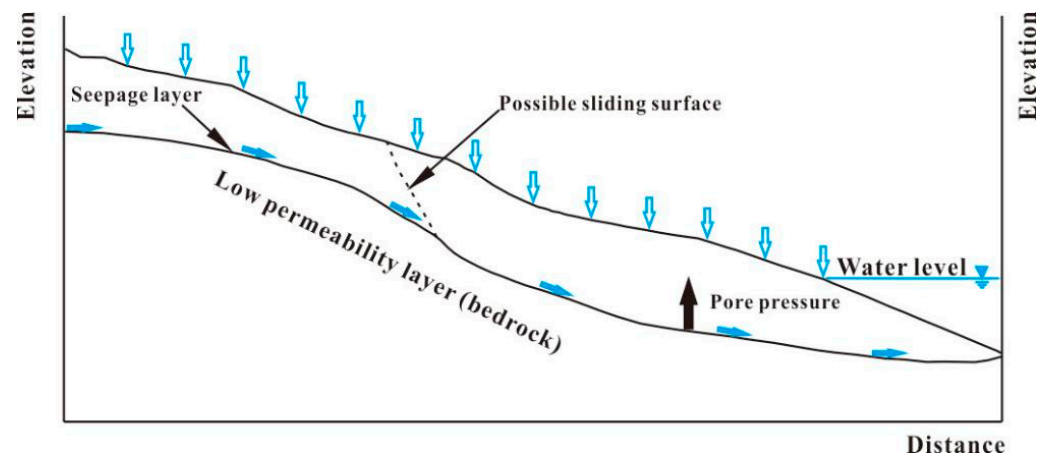


**Figure 19.** Conceptual model of a chair-shaped bedrock landslide under the conditions of lowering water levels and rainfall.

The significant pressure build-up and the rate of build-up were dependent on the rain intensity, elevation of the recharge zone, different properties of the upper and lower strata, and the rate at which the groundwater could escape from the toe of the slope. With the same conditions of rain intensity and recharge zone elevation, the properties of the strata and groundwater escape conditions were very important to the pore water pressure build-up. For example, if the rainfall on the exposed slope surface occurred at a rate less than the permeability of the slope materials, and the conditions at the toe of the slope were favorable for the ground water to escape, then the water may percolate vertically downwards into the slope without causing large positive pore water pressure level changes.

It was found that the properties between the upper and lower strata were quite different in the Zhaoshuling Landslide site. The bedrock was  $T_2b^2$  strata and had a permeability much lower than that of the slope material. The infiltrating water may have formed a seepage layer on the bedrock surface, which potentially followed the contours of the bedrock. Therefore, any significant change in the inclination of the bedrock may have resulted in localized changes in the hydraulic gradient. However, the bedrock of the Zhaoshuling Landslide was chair-shaped, with a particularly significant change in gradient in the toe region. Therefore, since the bedrock surface was slightly depressed and even upside down at the toe, the seepage flow was not smooth. A localized zone of high transient pore water pressure may have been created within the slope material, which could have potentially reduced the effective stress of the soil body. This was arguably the most critical region of the slope from a stress perspective. Therefore, it was believed that the investigated landslide event may have begun with a local slip under rainfall infiltration and reservoir water level change conditions.

## 6. Conclusions

It has been determined that rainfall and reservoir water fluctuations were significant factors inducing the failure of the Zhaoshuling Landslide. The shape of bedrock surface, and the pore water and total soil pressure levels in the landslide area were found to be sensitive to the presence of the water during the water lowering process and rainfall, which directly enhanced the displacements and may have even initiated the landslide failure. The following conclusions were drawn in the present research investigation:

1. The results obtained from this study's physical model tests indicated that the Zhaoshuling Landslide was stable when the reservoir water levels were fluctuating between 145 m and 175 m. However, rainstorm events combined with the quick decrease in

the reservoir water levels may have caused the toe of the landslide mass to fail, and the middle of the landslide mass to suffer large displacements.

2. It was revealed in this study that due to the bedrock surface shape of the Zhaoshuling Landslide, the deformations of the landslide area beneath an altitude of 300 m were more sensitive than those in the landslide areas located above that elevation. In the lower elevations, the pore water pressure had increased significantly, which adversely affected the stability of the slope.
3. A conceptual integrated model is put forward in this study to explain the failure mechanisms of the investigated landslide event. It was believed that the chair-shaped bedrock at the toe of the slope had significantly adverse effects on the mechanisms of the slope stability.

**Author Contributions:** Conceptualization, W.G. and R.H.; methodology, S.P. and W.G.; formal analysis, S.P. and W.G.; writing—original draft preparation, S.P.; investigation, S.P. and W.G.; writing—review and editing, S.P. and W.G.; supervision, R.H.; project administration, R.H. and W.G.; funding acquisition, W.G. All authors have read and agreed to the published version of the manuscript.

**Funding:** This research was funded by the National Natural Science Foundation of China, grant number 42007238; China Institute of Geological Environment Monitoring, grant number 0001212015CC60021. The APC was funded by the National Natural Science Foundation of China, grant number 42007238.

**Institutional Review Board Statement:** Not applicable.

**Informed Consent Statement:** Not applicable.

**Data Availability Statement:** Data is contained within the article.

**Acknowledgments:** The authors would like to acknowledge the financial support received from the National Natural Science Foundation of China (no. 42007238) and China Institute of Geological Environment Monitoring (no. 0001212015CC60021). The authors also appreciate the corporation received from Wu Jian and his students who assisted with the construction of the landslide model test system in China Three Gorges University.

**Conflicts of Interest:** The authors declare no conflict of interest.

## References

1. Chen, J.; Li, X.; Yang, Z. On the distribution and mechanism of landslides in the Three Gorges Reservoir area. *J. Eng. Geol.* **2005**, *13*, 305–309.
2. Huang, R. Large-scale landslides and their sliding mechanisms in China since the 20th century. *Chin. J. Rock Mech. Eng.* **2007**, *3*, 433–454. [[CrossRef](#)]
3. Wang, F.-W.; Zhang, Y.-M.; Huo, Z.-T.; Matsumoto, T.; Huang, B.-L. The July 14, 2003 Qianjiangping Landslide, Three Gorges Reservoir, China. *Landslides* **2004**, *1*, 157–162. [[CrossRef](#)]
4. Yin, Y.P.; Peng, X.M. Failure mechanism on Qianjiangping landslide in the Three Gorges Reservoir region. *Hydrogeol. Eng. Geol.* **2007**, 51–54. [[CrossRef](#)]
5. Jian, W.; Wang, Z.; Yin, K. Mechanism of the Anlesi Landslide in the Three Gorges Reservoir, China. *Eng. Geol.* **2009**, *108*, 86–95. [[CrossRef](#)]
6. Wang, H.; Xu, W.Y. Stability of Liangshuijing landslide under variation water levels of Three Gorges Reservoir. *Eur. J. Environ. Civ. Eng.* **2013**, *17*, s158–s177. [[CrossRef](#)]
7. Wang, Y.; Cheng, C.; He, G.; Zhang, Q. Landslide stability analysis based on random-fuzzy reliability: Taking Liangshuijing landslide as a case. *Stoch. Environ. Res. Risk Assess.* **2014**, *28*, 1723–1732. [[CrossRef](#)]
8. Shihabudheen, K.V.; Peethambaran, B. Landslide displacement prediction technique using improved neuro-fuzzy system. *Arab. J. Geosci.* **2017**, *10*, 502. [[CrossRef](#)]
9. He, K.; Li, X.; Yan, X.; Guo, D. The landslides in the Three Gorges Reservoir Region, China and the effects of water storage and rain on their stability. *Environ. Geol.* **2008**, *55*, 55–63. [[CrossRef](#)]
10. Du, J.; Yin, K.; Lacasse, S. Displacement prediction in colluvial landslides, Three Gorges Reservoir, China. *Landslides* **2013**, *10*, 203–218. [[CrossRef](#)]
11. Bordoni, M.; Meisina, C.; Valentino, R.; Lu, N.; Bittelli, M.; Chersich, S. Hydrological factors affecting rainfall-induced shallow landslides: From the field monitoring to a simplified slope stability analysis. *Eng. Geol.* **2015**, *193*, 19–37. [[CrossRef](#)]
12. Miao, F.; Wu, Y.; Li, L.; Tang, H.; Li, Y. Centrifuge model test on the retrogressive landslide subjected to reservoir water level fluctuation. *Eng. Geol.* **2018**, *245*, 169–179. [[CrossRef](#)]

13. Iqbal, J.; Dai, F.; Hong, M.; Tu, X.; Xie, Q. Failure Mechanism and Stability Analysis of an Active Landslide in the Xiangjiaba Reservoir Area, Southwest China. *J. Earth Sci.* **2018**, *29*, 646–661. [[CrossRef](#)]
14. Casadei, M.; Dietrich, W.E.; Miller, N.L. Testing a model for predicting the timing and location of shallow landslide initiation in soil-mantled landscapes. *Earth Surf. Processes Landf.* **2003**, *28*, 925–950. [[CrossRef](#)]
15. Chai, B.; Yin, K.; Du, J.; Xiao, L. Correlation between incompetent beds and slope deformation at Badong town in the Three Gorges Reservoir, China. *Environ. Earth Sci.* **2013**, *69*, 209–223. [[CrossRef](#)]
16. Miao, H.; Wang, G.; Yin, K.; Kamai, T.; Li, Y. Mechanism of the slow-moving landslides in Jurassic red-strata in the Three Gorges Reservoir, China. *Eng. Geol.* **2014**, *171*, 59–69. [[CrossRef](#)]
17. Jiao, J.J. A confined groundwater zone in weathered igneous rocks and its impact on slope stability. In Proceedings of the International Symposium on Hydrogeology and the Environment, Wuhan, China, 17–20 October 2000.
18. Freer, J.; McDonnell, J.J.; Beven, K.J.; Peters, N.E.; Burns, D.A.; Hooper, R.P.; Aulenbach, B.; Kendall, C. The role of bedrock topography on subsurface storm flow. *Water Resour. Res.* **2002**, *38*, 1269. [[CrossRef](#)]
19. Li, S.; Xu, Q.; Tang, M.; Qian, L.; Ren, J. Response patterns of old landslides with different slip-surface shapes triggered by fluctuation of reservoir water level. *J. Eng. Geol.* **2017**, *25*, 841–852.
20. Hu, R.; Wang, S. Main features and identification method of sliding-surface in soil and rock slopes. *J. Eng. Geol.* **2010**, *18*, 35–40.
21. Jia, G.; Zhan, T.L.; Chen, Y.; Fredlund, D. Performance of a large-scale slope model subjected to rising and lowering water levels. *Eng. Geol.* **2009**, *106*, 92–103. [[CrossRef](#)]
22. Uchimura, T.; Towhata, I.; Anh, T.T.L.; Fukuda, J.; Bautista, C.J.B.; Wang, L.; Seko, I.; Uchida, T.; Matsuoka, A.; Ito, Y.; et al. Simple monitoring method for precaution of landslides watching tilting and water contents on slopes surface. *Landslides* **2009**, *7*, 351–357. [[CrossRef](#)]
23. Fan, L.; Zhang, G.; Li, B.; Tang, H. Deformation and failure of the Xiaochatou Landslide under rapid drawdown of the reservoir water level based on centrifuge tests. *Bull. Eng. Geol. Environ.* **2017**, *76*, 891–900. [[CrossRef](#)]
24. Wang, F.; Dai, Z.; Zhang, S. Experimental study on the motion behavior and mechanism of submarine landslides. *Bull. Eng. Geol. Environ.* **2018**, *77*, 1117–1126. [[CrossRef](#)]
25. Wang, K.-L.; Lin, M.-L. Initiation and displacement of landslide induced by earthquake—A study of shaking table model slope test. *Eng. Geol.* **2011**, *122*, 106–114. [[CrossRef](#)]
26. Ni, P.; Wang, S.; Zhang, S.; Mei, L. Response of heterogeneous slopes to increased surcharge load. *Comput. Geotech.* **2016**, *78*, 99–109. [[CrossRef](#)]
27. Ma, J.; Tang, H.; Hu, X.; Bobet, A.; Yong, R.; Ez Eldin, M.A.M. Model testing of the spatial-temporal evolution of a landslide failure. *Bull. Eng. Geol. Environ.* **2017**, *76*, 323–339. [[CrossRef](#)]
28. Liu, S.; Zhang, S.; Li, J. Investigation of a landslide in the new site of Badong County by integrated geophysical survey. *Sci. China Ser. D-Earth Sci.* **2001**, *44*, 426–436. [[CrossRef](#)]
29. Luo, X.Q.; Sun, H.; Tham, L.G.; Junaideen, S.M. Landslide Model Test System and Its Application on the Study of Shiliushubao Landslide in Three Gorges Reservoir Area. *Soils Found.* **2010**, *50*, 309–317. [[CrossRef](#)]
30. Chen, L.X.; Yin, K.L.; Dai, Y.X. Building vulnerability evaluation in landslide deformation phase. *J. Mt. Sci.* **2011**, *8*, 286. [[CrossRef](#)]
31. Tang, H.M.; Hu, X.L.; Xiong, C.R. Stability prediction of Zhaoshuling landslide by physical model test. *Appl. Mech. Mater.* **2012**, *170–173*, 1147–1150. [[CrossRef](#)]
32. Liu, P.; Li, Z.; Hoey, T.; Kincal, C.; Zhang, J.; Zeng, Q.; Muller, J.-P. Using advanced InSAR time series techniques to monitor landslide movements in Badong of the Three Gorges Region, China. *Int. J. Appl. Earth Obs. Geoinf.* **2013**, *21*, 253–264. [[CrossRef](#)]
33. Shi, X.; Zhang, L.; Liao, M.; Balz, T. Deformation monitoring of slow-moving landslide with L-and C-band SAR interferometry. *Remote Sens. Lett.* **2014**, *5*, 951–960. [[CrossRef](#)]
34. Li, S.; Xu, Q.; Tang, M.; Iqbal, J.; Liu, J.; Zhu, X.; Liu, F.; Zhu, D. Characterizing the spatial distribution and fundamental controls of landslides in the Three Gorges Reservoir area, China. *Bull. Eng. Geol. Environ.* **2019**, *78*, 4275–4290. [[CrossRef](#)]
35. Tang, M.; Xu, Q.; Yang, H.; Li, S.; Iqbal, J.; Fu, X.; Huang, X.; Cheng, W. Activity law and hydraulics mechanism of landslides with different sliding surface and permeability in the Three Gorges Reservoir Area, China. *Eng. Geol.* **2019**, *260*, 105212. [[CrossRef](#)]